Neurobiology of Disease

Extracellular Zn^{2+} Is Essential for Amyloid β_{1-42}-Induced Cognitive Decline in the Normal Brain and Its Rescue

Atsushi Takeda,[1] Haruna Tamano,[1] Munekazu Tempaku,[1] Miku Sasaki,[1] Chihiro Uematsu,[1] Shoko Sato,[1] Hiroaki Kanazawa,[2] Zsolt L. Datki,[3] Paul A. Adlard,[4] and Ashley I. Bush[4]

[1]Department of Neurophysiology, School of Pharmaceutical Sciences, University of Shizuoka, Shizuoka 422-8526, Japan, [2]Department of Functional Anatomy, School of Nursing, University of Shizuoka, Shizuoka 422-8526, Japan, [3]Department of Psychiatry, University of Szeged, H-6726 Szeged, Hungary, and [4]Florey Institute of Neuroscience and Mental Health, University of Melbourne, Parkville, 3052 Victoria, Australia

Brain $A\beta_{1-42}$ accumulation is considered an upstream event in pathogenesis of Alzheimer's disease. However, accumulating evidence indicates that other neurochemical changes potentiate the toxicity of this constitutively generated peptide. Here we report that the interaction of $A\beta_{1-42}$ with extracellular Zn^{2+} is essential for *in vivo* rapid uptake of $A\beta_{1-42}$ and Zn^{2+} into dentate granule cells in the normal rat hippocampus. The uptake of both $A\beta_{1-42}$ and Zn^{2+} was blocked by CaEDTA, an extracellular Zn^{2+} chelator, and by Cd^{2+}, a metal that displaces Zn^{2+} for $A\beta_{1-42}$ binding. *In vivo* perforant pathway LTP was unaffected by perfusion with 1000 nM $A\beta_{1-42}$ in ACSF without Zn^{2+}. However, LTP was attenuated under preperfusion with 5 nM $A\beta_{1-42}$ in ACSF containing 10 nM Zn^{2+}, recapitulating the concentration of extracellular Zn^{2+}, but not with 5 nM $A\beta_{1-40}$ in ACSF containing 10 nM Zn^{2+}. $A\beta_{1-40}$ and Zn^{2+} were not taken up into dentate granule cells under these conditions, consistent with lower affinity of $A\beta_{1-40}$ for Zn^{2+} than $A\beta_{1-42}$. $A\beta_{1-42}$-induced attenuation of LTP was rescued by both CaEDTA and $CdCl_2$, and was observed even with 500 pM $A\beta_{1-42}$. $A\beta_{1-42}$ injected into the dentate granule cell layer of rats induced a rapid memory disturbance that was also rescued by coinjection of $CdCl_2$. The present study supports blocking the formation of Zn-$A\beta_{1-42}$ in the extracellular compartment as an effective preventive strategy for Alzheimer's disease.

Key words: $A\beta_{1-42}$; cognitive decline; dentate gyrus; extracellular Zn^{2+}

Significance Statement

Short-term memory loss occurs in normal elderly and increases in the predementia stage of Alzheimer's disease (AD). Amyloid-β_{1-42} ($A\beta_{1-42}$), a possible causing peptide in AD, is bound to Zn^{2+} in the extracellular compartment in the hippocampus induced short-term memory loss in the normal rat brain, suggesting that extracellular Zn^{2+} is essential for $A\beta_{1-42}$-induced short-term memory loss. The evidence is important to find an effective preventive strategy for AD, which is blocking the formation of Zn-$A\beta_{1-42}$ in the extracellular compartment.

Introduction

Cognitive function normally declines along with aging and is thought to be initially due to changes in synaptic function rather than loss of neurons (Morrison and Hof, 1997). Alzheimer's disease (AD) is the most common cause of dementia and has a preclinical phase of 20–30 years before clinical onset (Nestor et al., 2004; Querfurth and LaFerla, 2010). Amyloid-β ($A\beta$) accumulation in the neocortex, the hallmark pathology of AD, is thought to play an upstream role in disease pathogenesis. Through mechanisms that are uncertain, $A\beta$ oligomers can induce synapse dysfunction that contributes to cognitive decline in the predementia stage of AD (Perrin et al., 2009; Kepp, 2016).

$A\beta$ is normally produced in the brain, where the concentration has been estimated to be in the picomolar range in rodents (Cirrito et al., 2003). The peptide is prone to self-assembly into oligomers, protofibrils, and fibrils (Gu et al., 2016). $A\beta_{1-40}$ and $A\beta_{1-42}$ are the two most abundant isoforms. $A\beta_{1-40}$ is ≈10 times as abundant as $A\beta_{1-42}$ in biological fluids (Schoonenboom et al., 2005). Importantly, $A\beta_{1-42}$ far more readily forms aggregates and is more neurotoxic than $A\beta_{1-40}$ (Mucke et al., 2000).

$A\beta$ levels in the brain extracellular fluid are linked to cognitive activity (Cirrito et al., 2005; Puzzo et al., 2011). Synaptic vesicle release may be likely to be the primary mediator of dynamic changes in extracellular $A\beta$ levels, which in turn may modify

Received April 10, 2017; revised June 12, 2017; accepted June 19, 2017.

Author contributions: A.T. designed research; H.T., M.T., M.S., C.U., S.S., H.K., and Z.L.D. performed research; H.T. contributed unpublished reagents/analytic tools; A.T., H.T., P.A.A., and A.I.B. analyzed data; A.T. and A.I.B. wrote the paper.

The authors declare no competing financial interests.

Correspondence should be addressed to Dr. Atsushi Takeda, Department of Neurophysiology, School of Pharmaceutical Sciences, University of Shizuoka, 52-1 Yada, Suruga-ku, Shizuoka 422-8526, Japan. E-mail: takedaa@u-shizuoka-ken.ac.jp.

DOI:10.1523/JNEUROSCI.0954-17.2017

 0270-6474/17/377253-10$15.00/0

synaptic activity and are independent of changes in amyloid-β precursor protein (APP) processing (Cirrito et al., 2005). Studies of normal young animals report that endogenous Aβ is involved in learning and memory (Morley et al., 2010) ant that endogenous $A\beta_{1-42}$ supports LTP expression (Puzzo et al., 2011). Together, it is possible that $A\beta_{1-42}$ supports LTP and memory at picomolar concentrations under physiological conditions, whereas it impairs them at pathological nanomolar concentrations (Rammes et al., 2011; Puzzo et al., 2012).

Zn^{2+} has been implicated in the pathogenesis of AD by inducing Aβ oligomerization (Bush et al., 1994; Ayton et al., 2013; Bush, 2013). Here, we determine that $A\beta_{1-42}$ takes Zn^{2+} as a cargo into the dentate granule neurons in the normal brain causing LTP and memory impairment.

Materials and Methods

Animals and chemicals. Male Wistar rats (7–9 weeks of age) were purchased from Japan SLC. Rats were housed under the standard laboratory conditions (23 ± 1°C, 55 ± 5% humidity) and had access to tap water and food *ad libitum*. All the experiments were performed in accordance with the *Guidelines for the care and use of laboratory animals* of the University of Shizuoka that refer to the American Association for Laboratory Animals Science and the guidelines laid down by the National Institutes of Health *Guide for the care and use of laboratory animals*. The Ethics Committee for Experimental Animals in the University of Shizuoka has approved this work.

Synthetic human $A\beta_{1-42}$ and $A\beta_{1-40}$ were purchased from ChinaPeptides. Aβ was dissolved in saline and used immediately when the experiments were performed. SDS-PAGE showed that $A\beta_{1-42}$ prepared in saline was mainly monomers with a small fraction of low-order oligomers (Takeda et al., 2014a). ZnAF-2DA ($K_d = 2.7 \times 10^{-9}$ M for zinc), a membrane-permeable zinc indicator was kindly supplied by Sekisui Medical. ZnAF-2DA is taken up into the cells through the cell membrane and is hydrolyzed by esterase in the cytosol to yield ZnAF-2, which cannot permeate the cell membrane (Hirano et al., 2002; Ueno et al., 2002). Calcium Orange AM, a membrane-permeable calcium indicator, was purchased from Invitrogen. These fluorescence indicators were dissolved in DMSO and then diluted to ACSF containing 119 mM NaCl, 2.5 mM KCl, 1.3 mM $MgSO_4$, 1.0 mM NaH_2PO_4, 2.5 mM $CaCl_2$, 26.2 mM $NaHCO_3$, and 11 mM D-glucose, pH 7.3.

Hippocampal slice preparation. Wistar rats were anesthetized with ether and decapitated in accordance with the Japanese Pharmacological Society *Guide for the care and use of laboratory animals*. The brain was quickly removed and immersed in ice-cold choline-ACSF containing 124 mM choline chloride, 2.5 mM KCl, 2.5 mM $MgCl_2$, 1.25 mM NaH_2PO_4, 0.5 mM $CaCl_2$, 26 mM $NaHCO_3$, and 10 mM glucose, pH 7.3, to suppress neuronal excitation. Horizontal hippocampal slices (400 μm) were prepared in ice-cold choline-ACSF using a vibratome ZERO-1 (Dosaka) in an ice-cold choline-ACSF. Slices were then maintained in ACSF at 25°C for at least 30 min. All solutions used in the experiments were continuously bubbled with 95% O_2 and 5% CO_2.

In vitro *immunostaining.* Hippocampal slices were incubated with 50 μM $A\beta_{1-42}$ in ACSF, or with 50 μM $A\beta_{1-42}$ and either 50 μM metals or 500 μM CaEDTA in ACSF for 15 min. Slices were then washed twice with ACSF for 5 min to remove extracellular agents, and fixed with PFA (4% in 0.01 M PBS) for 15 min. Slices were rinsed in 0.01 M PBS three times. Tissues were then blocked in 10% normal goat serum for 30 min, rinsed in 0.01 M PBS three times, incubated with 70% formic acid for 5 min, rinsed with 0.01 M PBS three times, and incubated at 4°C with Aβ monoclonal antibody, 4G8 (Covance, 1:500 dilution in 0.01 M PBS) for 48 h. Slices were then rinsed with 0.01 M PBS three times, incubated with AlexaFluor-633 goat antimouse IgG secondary antibody (1: 200 dilution in 0.01 M PBS) for 1 h, rinsed in 0.01 M PBS three times, incubated with DAPI for 10 min, and then rinsed again with 0.01 M PBS three times before mounting on glass slides. Images for immunostaining were captured using a confocal laser-scanning microscopic system LSM 510 META (Carl Zeiss), equipped with an inverted microscope (Axiovert 200 M, Carl Zeiss) through a 10× and 40× objective. Florescence intensity was analyzed using National Institutes of Health ImageJ. The region of interest was set in the dentate granule cell layer in the dentate gyrus or in the pyramidal cell layer in the CA1 and CA3 subfields of the hippocampus.

In vivo *immunostaining.* Male rats were anesthetized with chloral hydrate (400 mg/kg) and placed in a stereotaxic apparatus. The skull was exposed, two burr holes were drilled, and injection cannulae (internal diameter, 0.15 mm; outer diameter, 0.35 mm) were bilaterally inserted into the dentate granule cell layer (4.0 mm posterior to the bregma, 2.3 mm

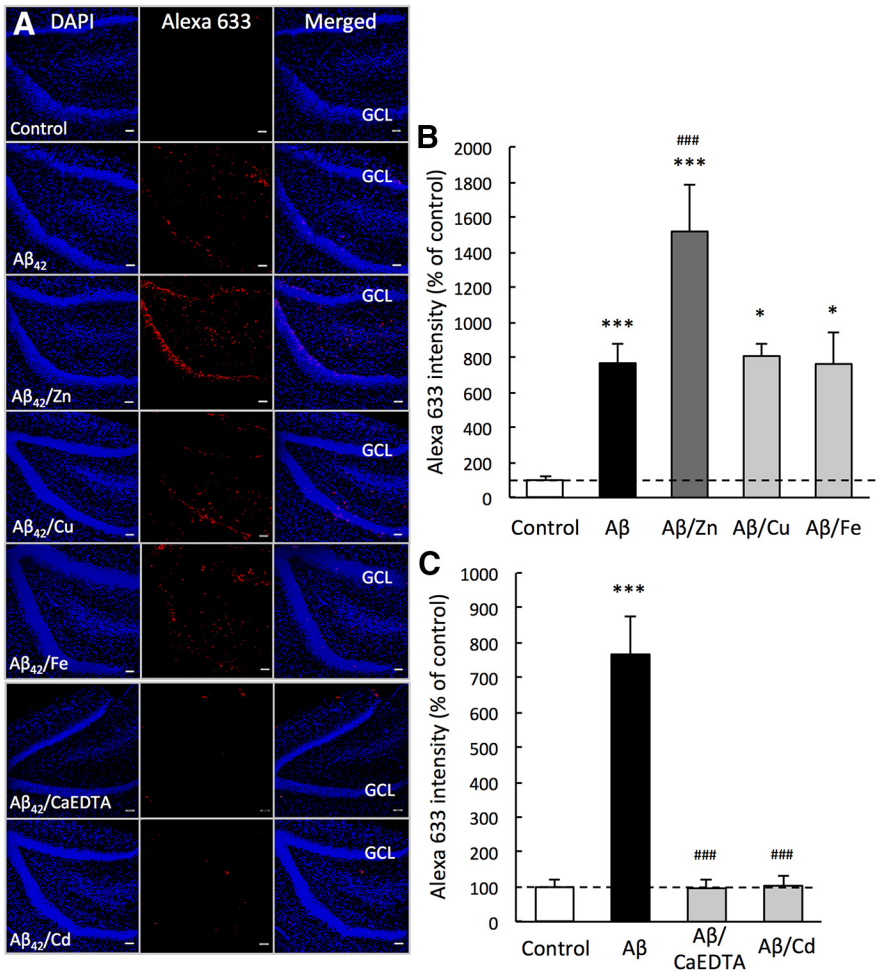

Figure 1. *In vitro* $A\beta_{1-42}$ uptake in the dentate gyrus. Hippocampal slices were incubated with 50 μM $A\beta_{1-42}$ in ACSF ($n = 29$), 50 μM $A\beta_{1-42}$ + 50 μM $ZnCl_2$ ($n = 27$), 50 μM $A\beta_{1-42}$ + 50 μM $CuCl_2$ ($n = 10$), 50 μM $A\beta_{1-42}$ + 50 μM $FeCl_3$ ($n = 9$), 50 μM $A\beta_{1-42}$ + 50 μM $CdCl_2$ ($n = 8$), or 50 μM $A\beta_{1-42}$ + 500 μM CaEDTA in ACSF ($n = 13$). ***A***, Aβ immunostaining in the dentate gyrus 15 min after incubation. GCL, Dentate granule cell layer. Scale bar, 50 μm. ***B***, ***C***, Aβ uptake in the dentate granule cell layer determined with Alexa-633 intensity, which is represented by the ratio to the control ($n = 32$) without 50 μM $A\beta_{1-42}$ in ACSF expressed as 100%. ***B***, $^{*}p < 0.05$ versus control. $^{***}p < 0.001$ versus control. $^{\#\#\#}p < 0.001$ versus Aβ. ***C***, $^{***}p < 0.001$ versus control. $^{\#\#\#}p < 0.001$ versus Aβ.

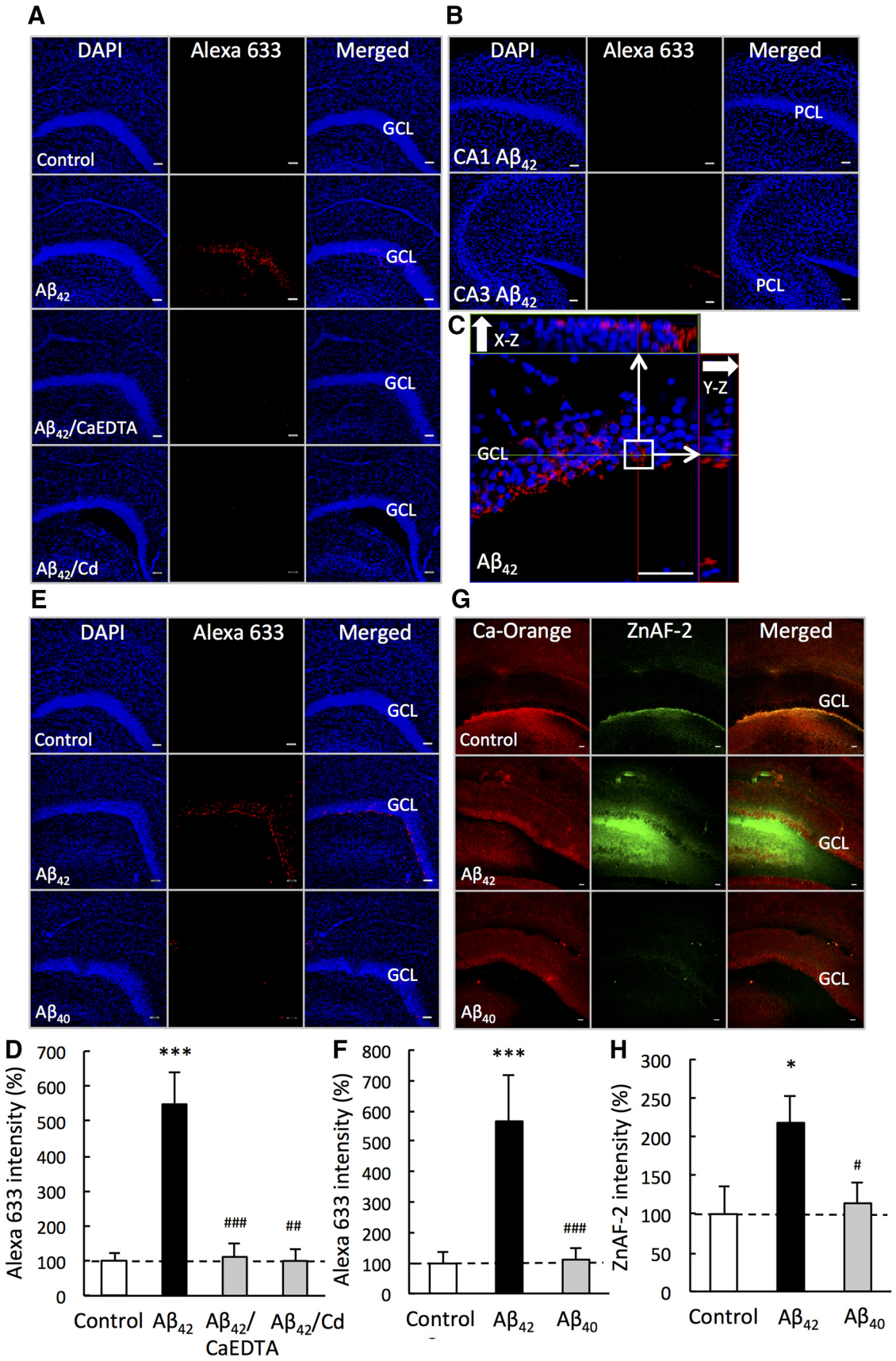

Figure 2. *In vivo* differential uptake of Aβ_{1-42} and Aβ_{1-40} in the dentate gyrus and involvement of Zn^{2+}. Fifty micromolar Aβ_{1-42} in ACSF ($n = 29$), 50 μM Aβ_{1-42} + 50 μM $CdCl_2$ in ACSF ($n = 10$), and 50 μM Aβ_{1-42} + 500 μM CaEDTA in ACSF ($n = 11$) were bilaterally injected via injection cannulae into the dentate granule cell layer of unanesthetized rats. ***A***, Aβ_{1-42} immunostaining in the dentate gyrus determined 5 min after injections. GCL, Dentate granule cell layer. Scale bar, 50 μm. ***B***, Aβ_{1-42} immunostaining in the CA1 and CA3 subfields 5 min after injection of 50 μM Aβ_{1-42} injection. PCL, Pyramidal cell layer. ***C***, Magnified image of Aβ_{1-42} in ***A***. ***D***, Aβ_{1-42} uptake in the dentate granule cell layer determined (*Figure legend continues.*)

lateral, 2.9 mm inferior to the dura). Thirty minutes later, following recovery from the insertion damage, 50 μM $A\beta_{1-42}$ in ACSF or 50 μM $A\beta_{1-42}$ with either 50 μM metals or 500 μM CaEDTA in ACSF was bilaterally injected via the injection cannulae into the dentate granule cell layer of unanesthetized rats at the rate of 0.25 μl/min for 8 min. Five minutes later, the brain was quickly removed as described above and immunostaining using hippocampal slices was performed in the same manner except for exchanging the 10% goat serum with 5% goat serum.

In vivo *intracellular Zn^{2+} imaging.* According to the procedure described above, ACSF containing 100 μM ZnAF-2DA was bilaterally injected via injection cannulae into the dentate granule cell layer of unanesthetized rats at the rate of 0.25 μl/min for 8 min. One hour later, 50 μM $A\beta_{1-42}$ in ACSF or 50 μM $A\beta_{1-42}$ + 50 μM metals in ACSF was bilaterally injected in the same manner. Five minutes later, the hippocampal slices were also prepared as noted above. In another experiment, 50 μM $A\beta_{1-42}$ in ACSF containing 100 μM ZnAF-2DA or 50 μM $A\beta_{1-42}$ + 500 μM CaEDTA in ACSF containing 100 μM ZnAF-2DA was bilaterally injected via injection cannulae into the dentate granule cell layer of unanesthetized rats at the rate of 0.25 μl/min for 8 min. The hippocampal slices were prepared in the same manner as above, transferred to a chamber filled with ACSF, loaded with 2 μM Calcium Orange AM in ACSF for 30 min to identify hippocampal regions, and then rinsed in ACSF for 10 min. The hippocampal slices were transferred to a recording chamber filled with ACSF. The fluorescence of ZnAF-2 (laser, 488 nm; emission, 505–530 nm) and Calcium Orange (laser, 543 nm; emission, >560 nm) was measured with a confocal laser-scanning microscopic system LSM 510.

In vivo *LTP.* Male rats were anesthetized with chloral hydrate (400 mg/kg) and placed in a stereotaxic apparatus. A bipolar stimulating electrode and a monopolar recording electrode made of tungsten wire attached to a microdialysis probe (AtmosLM, 1000 kDa cutoff, outer diameter 0.44 mm, Eicom) were positioned stereotactically so as to selectively stimulate the perforant pathway while recording under local perfusion with agents in ACSF (127 mM NaCl, 2.5 mM KCl, 0.9 mM $MgCl_2$, 1.0 mM NaH_2PO_4, 1.3 mM $CaCl_2$, 21 mM $NaHCO_3$, and 3.4 mM D-glucose, pH 7.3) at the rate of 1.0 μl/min in the dentate gyrus. The electrode stimulating the perforant pathway was positioned 8.0 mm posterior to the bregma, 4.5 mm lateral, 3.0–3.5 mm inferior to the dura. The recording electrode was implanted ipsilaterally 4.0 mm posterior to the bregma, 2.3–2.5 mm lateral and 3.0-3.5 mm inferior to the dura. All the stimuli were biphasic square wave pulses (200 μs width), and their intensities were set at the current that evoked 40% of the maximum population spike (PS) amplitude. Test stimuli (0.05 Hz) were delivered at 20 s intervals to monitor PS amplitude.

At the beginning of the experiments, input/output curves were generated by systematic variation of the stimulus current (0.1–1.0 mA) to evaluate synaptic potency. After stable baseline recording for at least 30 min, agents were added to the ACSF perfusate either before or after LTP induction. LTP was induced by delivery of high-frequency stimulation (10 trains of 20 pulses at 200 Hz separated by 1 s) and recorded for 60 min. PS amplitudes (test frequency: 0.05 Hz) were averaged over 120 s intervals and expressed as percentages of the mean PS amplitude measured during the 30 min baseline recordings, which was expressed as 100%. PS amplitudes for the last 10 min were also averaged and represented as the magnitude of LTP.

In another set of experiments, a bipolar stimulating electrode and a monopolar recording electrode made of tungsten wire attached to an injection cannula (internal diameter, 0.15 mm; outer diameter, 0.35 mm) were positioned stereotactically so as to selectively stimulate the perforant pathway while recording in the dentate gyrus. After stable baseline recording for at least 30 min, agents in 1 μl saline were locally injected into the dentate granule cell layer of anesthetized rats at the rate of 0.25 μl/min for 4 min via an injection cannula attached to a recording electrode. LTP was induced in the same manner.

Object recognition memory. The object recognition tests were performed in a separate cohort of animals. Briefly, rats were allowed to explore an open field (70 × 60 cm arena surrounded by 70 cm high walls, made of a black-colored plastic) for 10 min. Twenty-four hours later, agents in saline (1 μl) were bilaterally injected via injection cannulae into the dentate granule cell layer of unanesthetized rats at the rate of 0.25 μl/min for 4 min. One hour after injection, rats were trained and tested in a novel object recognition task. Training in the object recognition task took place in the same area used for the open field exploration. Thus, the open field exploration was used as a context habituation trial for the recognition memory task. The object recognition test requires that the rats recall which of two earthenware objects they had been previously familiarized with. Training was conducted by placing individual rats in the field, in which two identical objects (objects A1 and A2; sake bottle) were positioned in two adjacent corners, 15 cm from the walls. Rats were left to explore the objects for 5 min. Rats were not used for the test when the total of the object exploration time was <20 s. In the test given 1 h after training, the rats explored the open field for 3 min in the presence of one familiar (A) and one novel (B; cup) object. All objects were of similar texture, color, and size but were a distinctive shape (we confirmed that there was no preference for the objects used). All objects were washed with 70% ethanol between trials. The behavior of the rats was recorded with a video camera during the training and the test phases of the experiment, and then two people independently measured exploratory time and the averaged time was used. Exploration was defined as sniffing or touching the object with the nose and/or forepaws. A recognition index calculated for each rat was expressed by the ratio $T_B/(T_A + T_B)$, with T_A as time spent to explore the familiar object A and T_B as time spent to explore the novel object B.

Data analysis. For statistical analysis, Student's paired *t* test was used for comparison of the means of paired data. For multiple comparisons, differences between treatments were assessed by one-way ANOVA followed by *post hoc* testing using the Dunnett's test or the Tukey's test (the statistical software, GraphPad Prism 5). A value of $p < 0.05$ was considered significant. The Dunnett's test was used to compare between the control and treatments. The Tukey's test was used to compare between treatments in addition to the comparison between the control and treatments. Data are expressed as mean ± SE. The results of statistical analysis are described in each figure legend.

Results

Rapid hippocampal uptake of $A\beta_{1-42}$ is mediated by extracellular Zn^{2+}

Rat hippocampal slices were incubated for 15 min with $A\beta_{1-42}$, and peptide retention was determined by Aβ immunohistochemistry (monoclonal antibody 4G8). Aβ was observed to attach mainly in the dentate granule cell layer. The staining was markedly enhanced by coincubation with $ZnCl_2$, although it was not influenced by the presence of $CuCl_2$ and $FeCl_3$ (Fig. 1*A*,*B*). We then tested whether endogenous Zn^{2+} released from the hippocampal slices could be promoting $A\beta_{1-42}$ retention in the absence of additional extracellular Zn^{2+} (Takeda et al., 2017). Indeed, $A\beta_{1-42}$ retention was completely blocked in the presence of CaEDTA, an extracellular Zn^{2+} chelator (Fig. 1*A*,*C*). We confirmed that Zn^{2+} interaction with $A\beta_{1-42}$ was responsible for peptide retention in the absence of exogenous Zn^{2+} by displacing the endogenous Zn^{2+} released by the slices with Cd^{2+}, a non-physiological metal ion that competes with Zn^{2+} for the histidine

←

(*Figure legend continued.*) with Alexa-633 intensity, which is represented by the ratio to the control ($n = 28$) without 50 μM $A\beta_{1-42}$ in ACSF expressed as 100%. ***$p < 0.001$ versus control. ##$p < 0.01$ versus Aβ. ###$p < 0.001$ versus Aβ. ***E***, Aβ immunostaining images were determined in the dentate gyrus 5 min after bilateral injection of $A\beta_{1-42}$ ($n = 20$) and $A\beta_{1-40}$ ($n = 11$) (50 μM) in ACSF. ***F***, Aβ uptake in the dentate granule cell layer determined with Alexa-633 intensity, which is represented by the ratio to the control ($n = 28$) without 50 μM Aβ in ACSF expressed as 100%. ***$p < 0.001$ versus control. ###$p < 0.001$ versus $A\beta_{1-42}$. ***G***, Intracellular Zn^{2+} images were determined in the dentate gyrus 5 min after bilateral injection of $A\beta_{1-42}$ ($n = 15$) and $A\beta_{1-40}$ ($n = 19$) (50 μM) in ACSF containing 100 μM ZnAF-2DA. ***H***, Intracellular Zn^{2+} levels in the dentate granule cell layer determined with intracellular ZnAF-2, which is represented by the ratio to the control ($n = 6$) without 50 μM Aβ in ACSF expressed as 100%. *$p < 0.05$ versus control. #$p < 0.05$ versus $A\beta_{1-42}$.

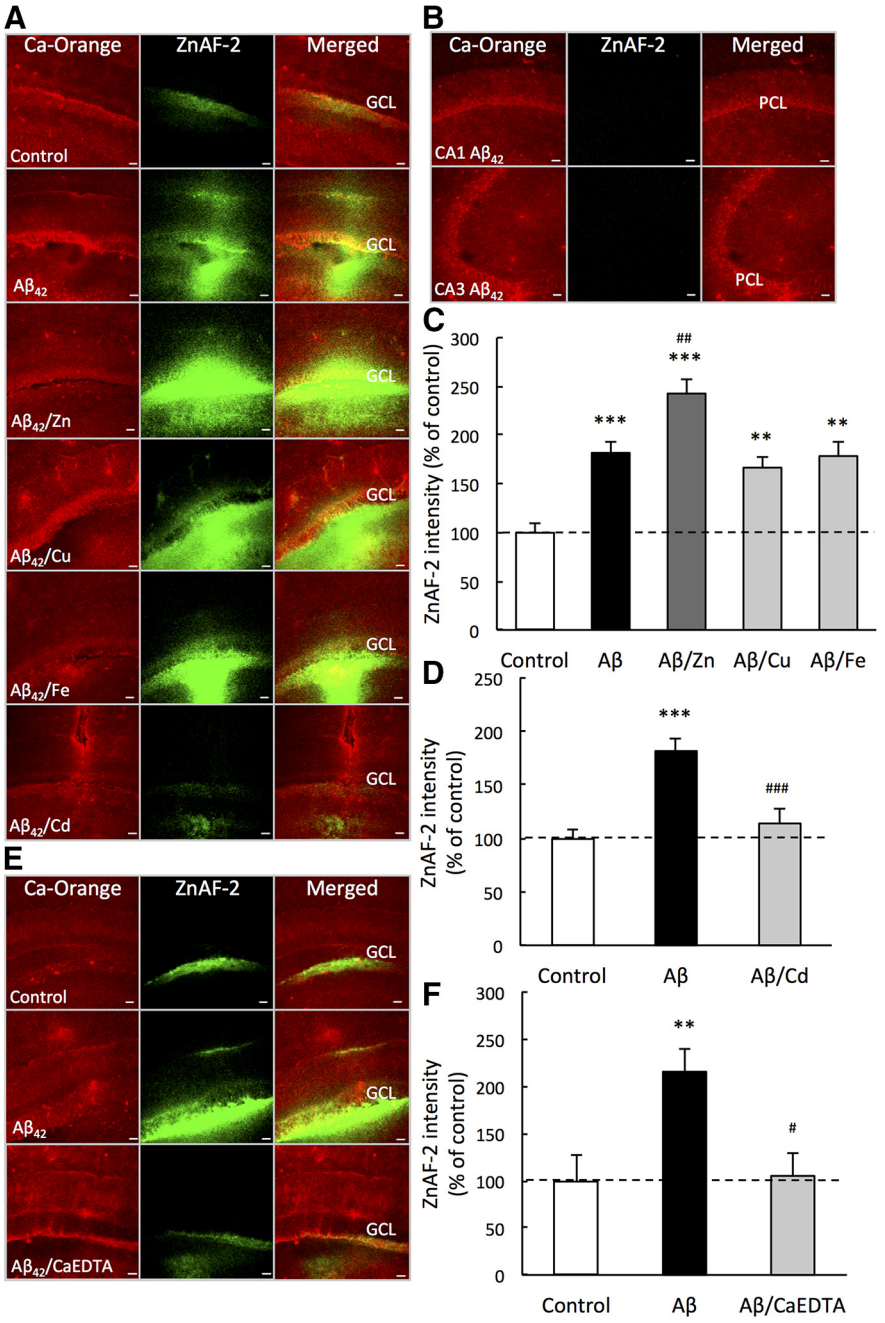

Figure 3. *In vivo* $A\beta_{1-42}$-mediated Zn^{2+} uptake in the dentate gyrus. ***A***, ACSF containing 100 μM ZnAF-2DA was bilaterally preinjected in the dentate gyrus to obtain intracellular ZnAF-2 images. One hour later, intracellular Zn^{2+} images were determined in the dentate gyrus 5 min after bilateral injection of 50 μM $A\beta_{1-42}$ in ACSF ($n = 13$), 50 μM $A\beta_{1-42}$ + 50 μM $ZnCl_2$ ($n = 11$), 50 μM $A\beta_{1-42}$ + 50 μM $CuCl_2$ ($n = 12$), 50 μM $A\beta_{1-42}$ + 50 μM $FeCl_3$ ($n = 11$), and 50 μM $A\beta_{1-42}$ + 50 μM $CdCl_2$ ($n = 11$) in ACSF. ***B***, Intracellular Zn^{2+} images were also determined in the CA1 and CA3 5 min after bilateral injection. ***C***, ***D***, Quantitation of intracellular Zn^{2+} levels in the dentate granule cell layer determined with intracellular ZnAF-2, which is represented by the ratio to the control ($n = 8$) without 50 μM $A\beta_{1-42}$ in ACSF expressed as 100%. $^{**}p < 0.01$ versus control. $^{***}p < 0.001$ versus control. $^{\#\#}p < 0.01$ versus $A\beta_{1-42}$. $^{\#\#\#}p < 0.001$ versus control. ***E***, Intracellular Zn^{2+} images were determined in the dentate gyrus 5 min after bilateral injection of 50 μM $A\beta_{1-42}$ ($n = 12$) and 50 μM $A\beta_{1-42}$ + 500 μM CaEDTA ($n = 8$) in ACSF containing 100 μM ZnAF-2DA. ***F***, Intracellular Zn^{2+} levels in the dentate granule cell layer determined in the same manner. $^{**}p < 0.01$ versus control ($n = 9$). $^{\#}p < 0.05$ versus $A\beta_{1-42}$.

residues of Aβ (Syme and Viles, 2006). $CdCl_2$ also abolished Aβ retention on the slices (Fig. 1*A*,*C*).

We studied the hippocampal retention of $A\beta_{1-42}$ *in vivo* by performing Aβ immunohistochemistry of the region captured 5 min after local injection of $A\beta_{1-42}$ into the dentate granule cell layer. $A\beta_{1-42}$ staining, which was also observed in the dentate granule cell layer, was observed around the nuclei of dentate granule cells (Fig. 2*A*,*C*,*D*), consistent with intracellular uptake. $A\beta_{1-42}$ staining was not observed in the CA1 and CA3 (Fig. 2*B*). $A\beta_{1-42}$ staining was completely blocked upon coinjection of CaEDTA and $CdCl_2$ (Fig. 2*A*,*D*). In contrast to $A\beta_{1-42}$, when $A\beta_{1-40}$ was injected, its retention in the hippocampus was not detectable in this time period (Fig. 2*E*,*F*).

Rapid hippocampal uptake of extracellular Zn^{2+} is mediated by $A\beta_{1-42}$

The *in vivo* status of intracellular Zn^{2+}, which was measured with ZnAF-2, was determined 5 min after local injection of $A\beta_{1-42}$ into the dentate granule cell layer. Intracellular ZnAF-2 fluorescence was increased after injection of $A\beta_{1-42}$, and the increase was enhanced after coinjection of $ZnCl_2$ (Fig. 3*A*,*C*). Intracellular ZnAF-2 fluorescence was not observed in the CA1 and CA3 (Fig. 3*B*), probably because there was no diffusion of ZnAF-2DA or $A\beta_{1-42}$ from the injection zone. $A\beta_{1-42}$-mediated increase in intracellular ZnAF-2 florescence was not influenced by coinjection of $CuCl_2$ or $FeCl_3$ (Fig. 3*A*,*C*) but blocked by coinjection of CaEDTA or $CdCl_2$ (Fig. 3*A*,*D*,*E*,*F*). Because CaEDTA does not enter the cell, we conclude that extracellular Zn^{2+} entering into the cell is the source of the increased ZnAF-2 fluorescence induced by $A\beta_{1-42}$.

In contrast to the effect of $A\beta_{1-42}$, local injection of $A\beta_{1-40}$ did not increase intracellular ZnAF-2 fluorescence (Fig. 2*G*,*H*).

$A\beta_{1-42}$-induced attenuation of LTP requires extracellular Zn^{2+}

We examined the impact of $A\beta_{1-42}$ drawing extracellular Zn^{2+} into the cell upon *in vivo* LTP in perforant pathway-dentate granule cell synapses, where the recording area was locally perfused with Aβ in ACSF. LTP was not attenuated upon perfusion with 5–1000 nM $A\beta_{1-42}$ (Fig. 4*A*). LTP was not attenuated upon perfusion with ACSF containing 10 nM $ZnCl_2$ (representing the concentration of extracellular Zn^{2+}) (Frederickson et al., 2006) but was significantly attenuated upon perfusion with 5 nM $A\beta_{1-42}$ in ACSF containing 10 nM $ZnCl_2$ (Fig. 4*B*). LTP was also attenuated by the preperfusion with 5 nM $A\beta_{1-42}$ in ACSF containing 10 nM $ZnCl_2$ before tetanic stimulation, but not by the perfusion during and after tetanic stimulation (Fig. 4*C*). In the absence of $A\beta_{1-42}$, LTP was not attenuated by preperfusion with 100 nM $ZnCl_2$, but continuous perfusion with 100 nM $ZnCl_2$ did attenuate LTP (Fig. 5*A*). The preperfusion of 5 nM $A\beta_{1-42}$ with 10 nM $CuCl_2$, $FeCl_3$, or $CdCl_2$ instead of $ZnCl_2$

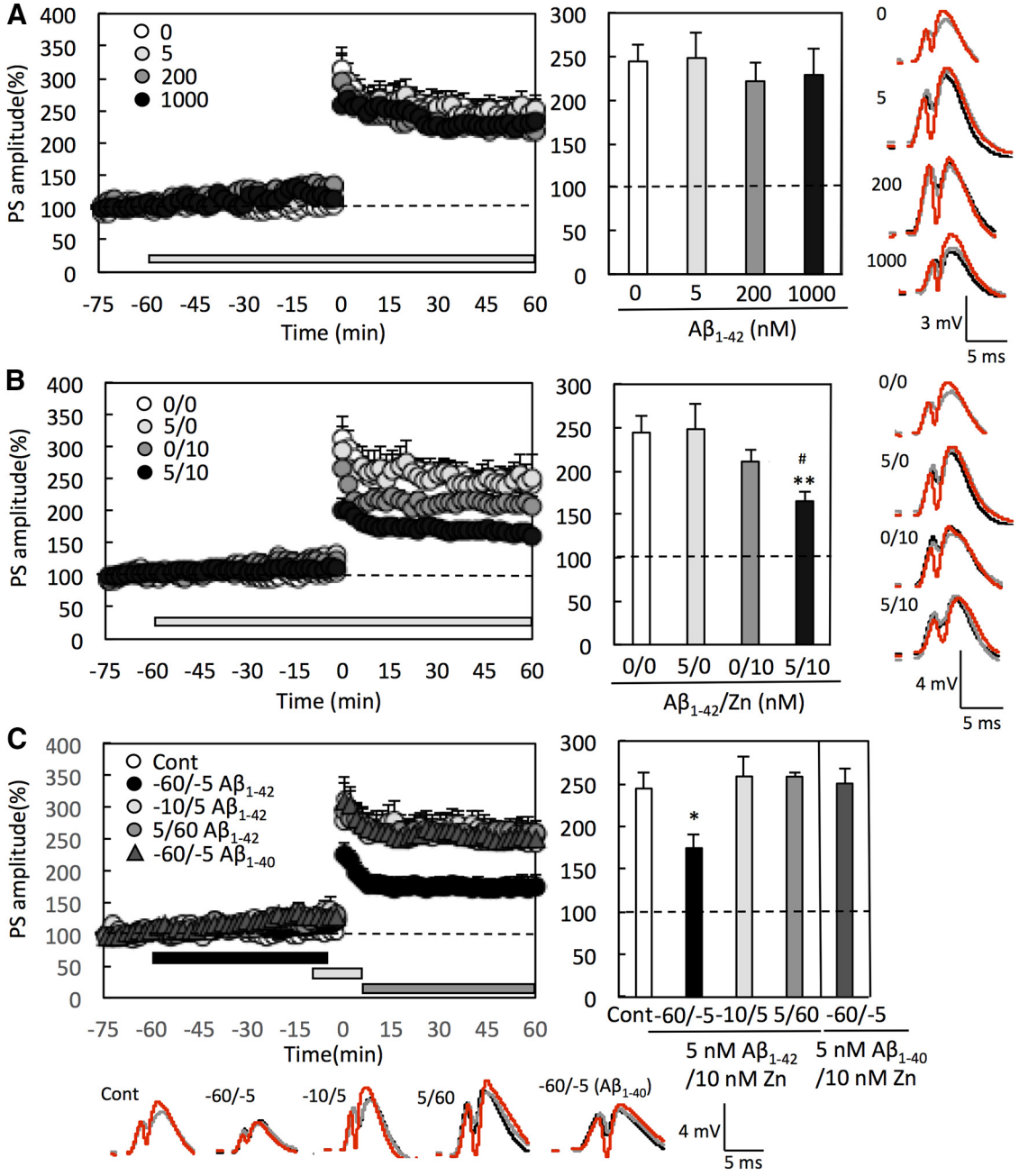

Figure 4. Involvement of extracellular Zn^{2+} in $A\beta_{1-42}$-induced attenuation of LTP. ***A***, Recording region was perfused with either ACSF ($n = 9$) or 5 ($n = 5$), 200 ($n = 6$), or 1000 nM $A\beta_{1-42}$ ($n = 7$) in ACSF for 60 min. High-frequency stimulation (10 trains of 20 pulses at 200 Hz separated by 10 s) was delivered at time 0 min and perfused for 60 min under the same condition. Left, PS amplitude over time. Bar represents the perfusion period with $A\beta$. Middle panels, Average PS amplitude (mean ± SEM) during the last 10 min of recording. Right, Representative fEPSP traces with PS recordings at the time −70 min (gray), −30 min (black), and 50–60 min (red). ***B***, Left, LTP was induced in the same manner under perfusion with 5 nM $A\beta_{1-42}$ ($n = 5$), 10 nM $ZnCl_2$ ($n = 7$), and 5 nM $A\beta_{1-42}$ + 10 nM $ZnCl_2$ ($n = 11$). Middle panels, Average PS amplitude (mean ± SEM) during the last 10 min of recording. Right, Representative fEPSP traces with PS recordings at the time −70 min (gray), −30 min (black), and 50–60 min (red). $^{**}p < 0.001$ versus control (0/0) ($n = 9$). $^{\#}p < 0.05$ versus 5 nM $A\beta_{1-42}$. ***C***, LTP was induced under differential perfusion period (−60 to −5 min, $n = 8$; −10 to 5 min, $n = 5$; 5 to 60 min, $n = 5$) with 5 nM $A\beta_{1-42}$ + 10 nM $ZnCl_2$ and also induced under preperfusion (−60 to −5 min) with 5 nM $A\beta_{1-40}$ + 10 nM $ZnCl_2$ ($n = 8$). Left, Bars represent the perfusion period. Middle, Each bar (mean ± SEM) represents the averaged PS amplitude of the last 10 min of recording. Right, LTP was attenuated under preperfusion with 5 nM $A\beta_{1-42}$ + 10 nM $ZnCl_2$, but not with 5 nM $A\beta_{1-40}$ + 10 nM $ZnCl_2$. Bottom, Representative fEPSP with PS recordings at the time −70 min (gray), −30 min (black), and 50–60 min (red). $^{*}p < 0.05$ versus control ($n = 11$).

did not attenuate LTP (Fig. 5*B*). On the other hand, the attenuation of LTP seen with 5 nM $A\beta_{1-42}$ in ACSF containing 10 nM $ZnCl_2$ was rescued when 1 mM CaEDTA or 10 nM $CdCl_2$ was added to the perfusate (Fig. 5*C*). LTP was not attenuated under preperfusion with 5 nM $A\beta_{1-40}$ in ACSF containing 10 nM $ZnCl_2$ (Fig. 4*C*).

$A\beta_{1-42}$-induced short-term memory decline is rescued by Cd^{2+}

LTP was attenuated 1 h after local injection of $A\beta_{1-42}$ (25 μM, 1 μl) into the dentate granule cell layer (control, 230 ± 7%; $A\beta_{1-42}$, 174 ± 9%, $p < 0.001$ vs control) and the attenuation was rescued by coinjection of $CdCl_2$ (50 μM, 226 ± 9%, $p < 0.05$ vs $A\beta_{1-42}$)

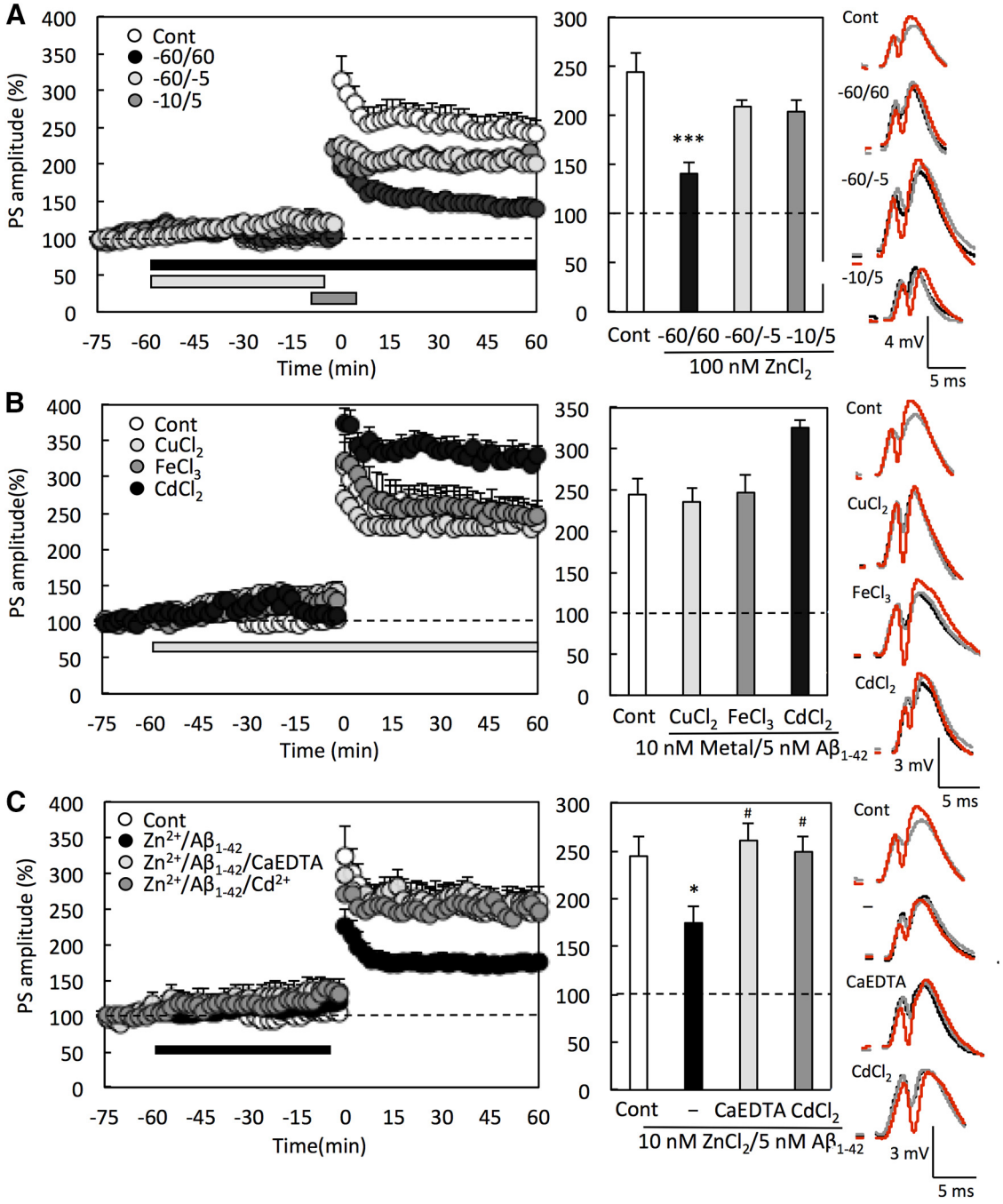

Figure 5. Rescue of $A\beta_{1-42}$- and Zn^{2+}-induced attenuation of LTP in the presence of CaEDTA and $CdCl_2$. ***A***, LTP was induced under differential perfusion period (−60 to 60 min, $n = 9$; −60 to −5 min, $n = 5$; −10 to 5 min, $n = 7$) with 100 nM $ZnCl_2$ in ACSF. Left, Bars represent the perfusion period. Middle, Each bar (mean ± SEM) represents the averaged PS amplitude of the last 10 min. LTP was not significantly attenuated under preperfusion with 100 nM $ZnCl_2$. Right, Representative fEPSP with PS recordings at the time −70 min (gray), −30 min (black), and 50–60 min (red). $^{***}p < 0.001$ versus control ($n = 11$). ***B***, LTP was induced under preperfusion with 5 nM $A\beta_{1-42}$ + 10 nM $CuCl_2$ ($n = 5$), 5 nM $A\beta_{1-42}$ + 10 nM $FeCl_3$ ($n = 4$), and 5 nM $A\beta_{1-42}$ + 10 nM $CdCl_2$ ($n = 5$) in ACSF. Left, Bar represents the perfusion period. Middle, Each bar and line (mean ± SEM) indicate the averaged PS amplitude of the last 10 min. Right, Representative fEPSP with PS recordings at the time −70 min (gray), −30 min (black), and 50–60 min (red). ***C***, LTP was induced under preperfusion with 5 nM $A\beta_{1-42}$ + 10 nM $ZnCl_2$ ($n = 8$), 5 nM $A\beta_{1-42}$ + 10 nM $ZnCl_2$ + 1 mM CaEDTA ($n = 5$), and 5 nM $A\beta_{1-42}$ + 10 nM $ZnCl_2$ + 10 nM $CdCl_2$ ($n = 7$) in ACSF. Left, Bar represents the perfusion period. Middle, Each bar and line (mean ± SEM) indicate the averaged PS amplitude of the last 10 min. Right, Representative fEPSP with PS recordings at the time −70 min (gray), −30 min (black), and 50–60 min (red). $^{*}p < 0.05$ versus control ($n = 11$). $^{\#}p < 0.05$ versus 5 nM $A\beta_{1-42}$ + 10 nM $ZnCl_2$.

(Fig. 6*A*), consistent with Cd^{2+} displacing Zn^{2+} from Aβ in the slice experiments (Fig. 3*D*). The novel object recognition test was then performed 1 h after local injection of $A\beta_{1-42}$ in the same manner (exploring time, control, 44.2 ± 13.8 s; $A\beta_{1-42}$, 51.8 ± 2.8 s; $A\beta_{1-42}$/Cd, 50.1 ± 5.4 s; Cd, 44.6 ± 4.6 s). One hour later, object recognition memory was impaired in the animals injected with $A\beta_{1-42}$, whereas the impairment was rescued by coinjection of $CdCl_2$ (Fig. 6*B*). LTP and object recognition memory were not impaired by injection of $CdCl_2$ alone.

Finally, the action of $A\beta_{1-42}$ in LTP induction was assessed under local perfusion of the animal at the concentrations of <1 nM. LTP was significantly attenuated under preperfusion with 500 pM $A\beta_{1-42}$ in

ACSF containing 10 nM $ZnCl_2$, but not with 100 pM $A\beta_{1-42}$ in ACSF containing 10 nM $ZnCl_2$ (Fig. 6*C*).

Discussion

It is reported that the concentrations of zinc, copper, and iron in the human CSF are 0.38, 0.34, and 0.54 μM, respectively (Gellein et al., 2008; Michalke and Nischwitz, 2010). Although the concentrations of these metals are unknown in the brain extracellular fluid, a fraction is exchangeable. It is reported that Aβ is bound to Zn^{2+} via histidine residues and that the K_d values of Zn^{2+} to $A\beta_{1-40}$ are in the range of 0.1–60 μM (Tõugu et al., 2008). However, the K_d value of Zn^{2+} to $A\beta_{1-42}$ is unreported. It is likely that, as is the case with Cu^{2+} binding to Aβ (Atwood et al., 2000), the apparent K_d of metal binding to $A\beta_{1-42}$ is higher in affinity than to $A\beta_{1-40}$ probably due to the perturbed equilibrium caused by the increased self-assembly of $A\beta_{1-42}$ oligomers. *In vivo* LTP at medial perforant pathway-dentate granule cell synapses, which is closely linked to object recognition memory (Takeda et al., 2014a, b; Suzuki et al., 2015), was not affected by perfusion with 1000 nM $A\beta_{1-42}$ in ACSF without Zn^{2+}, but attenuated under preperfusion with 5 nM $A\beta_{1-42}$ in ACSF containing 10 nM Zn^{2+}, as estimated Zn^{2+} concentration in the brain extracellular compartment under the basal (static) conditions (Frederickson et al., 2006). The attenuation was rescued by extracellular Zn^{2+} chelation with CaEDTA, whereas the attenuation was not observed under preperfusion with 5 nM $A\beta_{1-40}$ in ACSF containing 10 nM Zn^{2+}. These data indicate that low nanomolar $A\beta_{1-42}$, unlike $A\beta_{1-40}$, rapidly binds extracellular Zn^{2+} and subsequently attenuates LTP, consistent with subsequent object recognition memory decline. Thus, extracellular Zn^{2+} may impact on $A\beta_{1-42}$-induced cognitive decline via attenuated LTP in the normal brain.

When $A\beta_{1-42}$ was added to hippocampal slices, its uptake into dentate granule cells was increased in ACSF-containing Zn^{2+}, whereas it was blocked in ACSF containing CaEDTA. *In vivo* rapid $A\beta_{1-42}$ uptake into dentate granule cells was also completely blocked by coinjection of $A\beta_{1-42}$ with CaEDTA into the dentate gyrus. Simultaneously, *in vivo* rapid Zn^{2+} uptake into dentate granule cells, which was induced by injection of $A\beta_{1-42}$, was completely blocked by coinjection of CaEDTA. Together, our findings indicate that the interaction of $A\beta_{1-42}$ with extracellular Zn^{2+} promotes uptake of $A\beta_{1-42}$ into dentate granule cells in the normal brain, causing an increase in intracellular Zn^{2+}, and leading rapidly to cognitive impairment (Fig. 7). Preclinical and clinical data show the potential for metal chelation-based drug therapy for AD: Clioquinol reduces zinc accumulation in neuritic plaques and inhibits the amyloidogenic pathway in the APP/PS1 transgenic mouse brain (Wang et al., 2012). Clioquinol also promotes the degradation of metal-dependent Aβ oligomers to restore endocytosis and ameliorates Aβ toxicity (Matlack et al., 2014). Furthermore, PBT2, a copper/zinc ionophore and second-generation 8-hydroxyquinoline analog, significantly lowers Aβ levels in the CSF and improves cognitive performance over baseline in several key executive function tests (Lannfelt et al., 2008; Faux et al., 2010). Zn^{2+}- or Cu^{2+}-induced aggregates of Aβ (i.e., soluble oligomers) have been implicated as the neurotoxic form of the peptides against synapse function and structure.

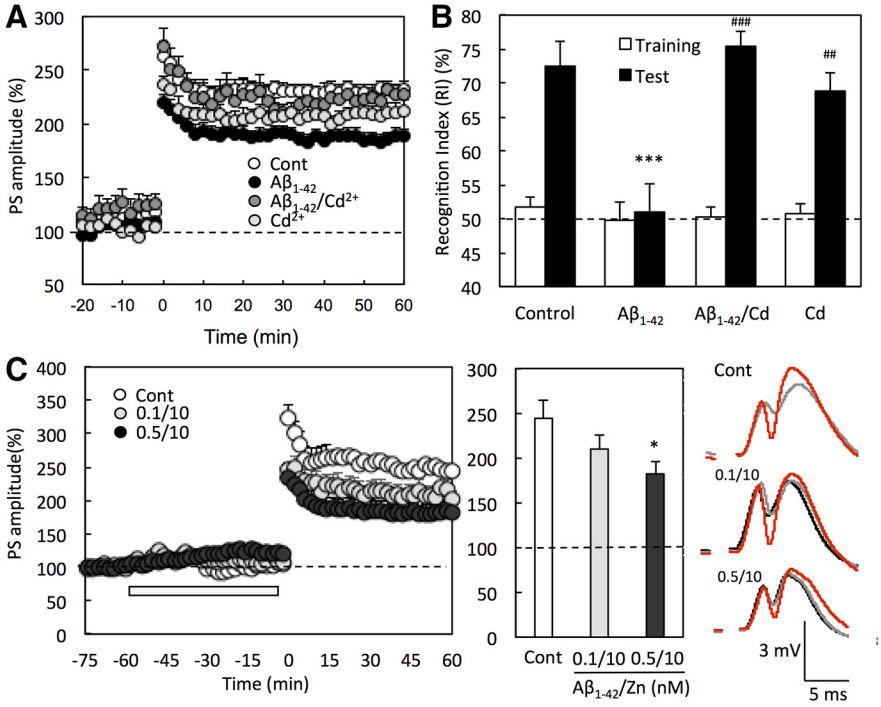

Figure 6. Rescue of $A\beta_{1-42}$-induced impairments of LTP and memory in the presence of $CdCl_2$ and picomolar $A\beta_{1-42}$-induced attenuation of LTP. ***A***, LTP was induced 1 h after injection of 25 μM $A\beta_{1-42}$ ($n = 18$), 25 μM $A\beta_{1-42}$ + 50 μM $CdCl_2$ ($n = 5$), and 50 μM $CdCl_2$ ($n = 6$) in ACSF (1 μl) via an injection cannula into the dentate granule cell layer (time 0 min). LTP was significantly ($p < 0.001$ vs control; $n = 24$) attenuated by coinjection of $A\beta_{1-42}$, and the attenuation was significantly ($p < 0.05$ vs $A\beta_{1-42}$) rescued by coinjection of $CdCl_2$. ***B***, Training of object recognition test was performed 1 h after bilateral injection of 25 μM $A\beta_{1-42}$ ($n = 9$), 25 μM $A\beta_{1-42}$ + 50 μM $CdCl_2$ ($n = 9$), and 50 μM $CdCl_2$ ($n = 8$) (1 μl) in ACSF into the dentate granule cell layer. One hour later, the test was performed. $^{***}p < 0.001$ versus control ($n = 10$). $^{\#\#}p < 0.01$ versus $A\beta_{1-42}$. $^{\#\#\#}p < 0.001$ versus $A\beta_{1-42}$. Recognition indices in the test were significantly elevated in the control ($p < 0.001$, *t* test), $A\beta_{1-42}$/Cd ($p < 0.001$, *t* test), and Cd ($p < 0.01$, *t* test) groups. ***C***, LTP was induced under preperfusion with 100 pM $A\beta_{1-42}$ + 10 nM $ZnCl_2$ ($n = 5$) and 500 pM $A\beta_{1-42}$ + 10 nM $ZnCl_2$ ($n = 11$) in ACSF. Bar represents the perfusion period (left). Scale bar and line (mean ± SEM) indicate the averaged PS amplitude of the last 10 min (middle). Representative fEPSP with PS recordings at the time −70 min (gray), −30 min (black), and 50–60 min (red) (right). $^{*}p < 0.05$ versus control ($n = 11$).

The medial perforant pathway is nonzincergic and does not release Zn^{2+} (Sindreu et al., 2003). Extracellular Zn^{2+} concentration at medial perforant pathway-dentate granule cell synapses may be relatively static in the hippocampus and may be maintained at ~10 nM (Frederickson et al., 2006). Such rapid uptake into dentate granule cells was not observed after injection of $A\beta_{1-40}$, probably due to less interaction of low nanomolar $A\beta_{1-40}$ with Zn^{2+} in the extracellular compartment. Hence, $A\beta_{1-40}$ perfusion had little effect on LTP induction. Increasing evidence has suggested that formation and propagation of misfolded aggregates of $A\beta_{1-42}$, rather than of $A\beta_{1-40}$, contribute to AD pathogenesis. However, structural details of misfolded $A\beta_{1-42}$ remain to be clarified (Ahmed et al., 2010). Masuda et al. (2009) report that C-terminal carboxylate anion of $A\beta_{1-42}$ forms the C-terminal hydrophobic core that accelerates neurotoxic oligomerization. Xiao et al. (2015) report that C-terminal Ala42, absent in $A\beta_{1-40}$, forms a salt bridge with Lys28 to create a self-recognition molecular switch that is the $A\beta_{1-42}$-selective self-replicating amyloid-propagation

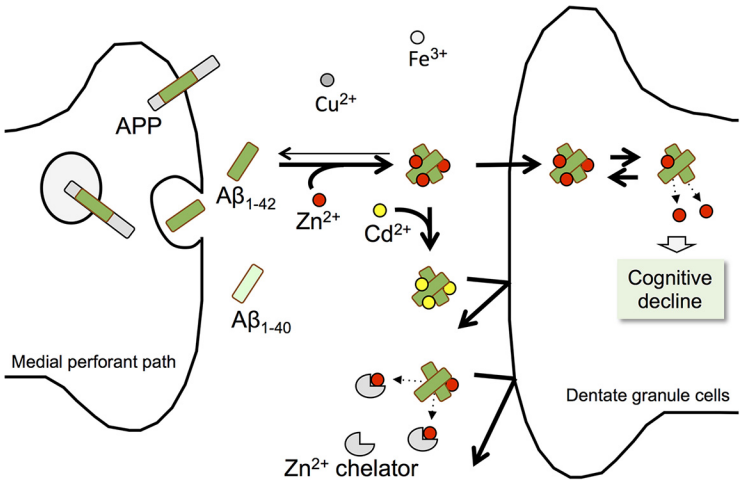

Figure 7. A model for neuronal intoxication by Zn-$A\beta_{1-42}$ complexes. Dentate granule cells will only take up $A\beta_{1-42}$ when it is bound to Zn^{2+}, whereupon Zn-$A\beta_{1-42}$ complexes enter neurons and either the complexes or the liberated Zn^{2+} induces cognitive decline via attenuated LTP. Cd^{2+}, but not Cu^{2+} or Fe^{3+}, can displace Zn^{2+} from $A\beta_{1-42}$ and prevent it from being taken up into granule cells, neutralizing its toxicity. Zn^{2+} is withdrawn into peptide complexes more readily by oligomers; hence, $A\beta_{1-42}$, which more rapidly forms oligomers, fosters neuronal uptake more readily than $A\beta_{1-40}$.

machinery. The aggregation property of $A\beta_{1-42}$ is promoted with Zn^{2+}, resulting in higher affinity of $A\beta_{1-42}$ to Zn^{2+} than $A\beta_{1-40}$ that leads to synaptic dysfunction via neuronal Zn-$A\beta_{1-42}$ uptake.

$A\beta$ can bind up to 3.5 equivalents of Zn^{2+} and Cu^{2+} simultaneously (Atwood et al., 2000) and can bind several other transition metals. However, at pH 7.4, only Zn^{2+}, but not Cu^{2+}, causes significant $A\beta$ aggregation. The reversible oligomerization of $A\beta$ induced by Zn^{2+} forming salt-bridges between peptide subunits (Huang et al., 1997) may be the physical basis for our observations that Cu^{2+} and Fe^{3+} do not compete for Zn^{2+} uptake into cells. $A\beta_{1-40}$ possesses selective affinity Cu^{2+} binding sites, and the binding affinity of Cu^{2+} is greater than for Zn^{2+}. If Cu^{2+} is preferentially bound to $A\beta_{1-42}$ in the extracellular compartment, it blocks $A\beta_{1-42}$-mediated Zn^{2+} accumulation. $CuCl_2$ (50 μM) did not modify *in vitro* $A\beta_{1-42}$ uptake into dentate granule cells, which might be mediated by endogenous Zn^{2+} released from the hippocampal slices (Takeda et al., 2017). Furthermore, *in vivo* increase in $A\beta_{1-42}$-mediated Zn^{2+} uptake into dentate granule cells was not modified by coinjection of $A\beta_{1-42}$ and $CuCl_2$ (50 μM). These data suggest that extracellular Zn^{2+} is bound to $A\beta_{1-42}$ even in the presence of micromolar Cu^{2+} and Fe^{3+} at neutral pH, resulting in the increase in intracellular Zn^{2+}. Because ZnAF-2 (K_d, 2.7 nM) must have a higher affinity than $A\beta_{1-42}$ for Zn^{2+}, it is estimated that *in vivo* K_d value of Zn^{2+} to $A\beta_{1-42}$ is in the range of ~3–30 nM. The free intracellular Zn^{2+} concentration is estimated to be <1 nM (Sensi et al., 1997; Colvin et al., 2008). Therefore, once ferried by $A\beta_{1-42}$ into dentate granule cells, the Zn^{2+} cargo is released in dentate granule cells. This may be critical for $A\beta_{1-42}$-induced cognitive decline in the normal rats. Because Zn^{2+} has many potential targets in dentate granule cells, the mechanism of the Zn^{2+} neurotoxicity is complex. Zhang et al. (2008) report abundant expression of Zn^{2+} transporters in the amyloid plaques of AD brain. Altered protein levels of the membrane Zn^{2+} transporters ZnT1, ZnT4, and ZnT6 have been reported in AD postmortem brain tissue (Beyer et al., 2012). The evidence suggests that Zn^{2+} transporters are involved in the pathological processes that lead to plaque formation. In a short period when the Zn^{2+} neurotoxicity is induced in the present study, however, the involvement of Zn^{2+} transporters might be modest.

In contrast, both $A\beta_{1-42}$ uptake and intracellular Zn^{2+} increase were blocked by Cd^{2+}. Together, these data are consistent with the possibility that $A\beta_{1-42}$ preferentially enters the cell when it forms a complex with Zn^{2+}, and that Cu^{2+} and Fe^{3+} are unable to compete off the Zn^{2+} entirely, whereas Cd^{2+} can. Thus, the neuronal dysfunction that we observed would be mediated by the intrusion of $A\beta$, Zn^{2+}, or both together (Fig. 7).

It is reported that the mean concentration of $A\beta_{1-42}$ in the CSF is significantly reduced in subjects with Alzheimer's disease compared with age-matched controls and is ~500 pM in age-matched controls (Motter et al., 1995). On the other hand, 200 pM human $A\beta_{1-42}$ improves LTP and memory in normal mice (Puzzo et al., 2008) and in mice challenged with antirodent $A\beta$ monoclonal antibody and siRNA against murine APP (Puzzo et al., 2011). In the hippocampus of young mice, extracellular $A\beta$ concentration measured by microdialysis is ~160 pM and extracellular $A\beta_{1-42}$ is ~20 pM, and not significantly changed in aged mice (Cirrito et al., 2003). Synaptic activity increases both extracellular $A\beta_{1-42}$ (Cirrito et al., 2005; Kim et al., 2010) and extracellular Zn^{2+} at zincergic synapses (Takeda and Tamano, 2016). So we hypothesize that a decrease in clearance mechanisms may lead to the inappropriate combination of Zn^{2+} with $A\beta_{1-42}$, leading to a toxic aggregate that enters neurons.

In conclusion, Zn^{2+} induces $A\beta_{1-42}$ uptake in the normal dentate gyrus, and memory dysfunction, when extracellular $A\beta_{1-42}$ reaches high picomolar concentrations. Blocking the formation of Zn-$A\beta_{1-42}$ in the extracellular compartment may be an effective strategy for preventing $A\beta_{1-42}$-mediated cognitive decline.

References

Ahmed M, Davis J, Aucoin D, Sato T, Ahuja S, Aimoto S, Elliott JI, Van Nostrand WE, Smith SO (2010) Structural conversion of neurotoxic amyloid-beta(1–42) oligomers to fibrils. Nat Struct Mol Biol 17:561–567. CrossRef Medline

Atwood CS, Scarpa RC, Huang X, Moir RD, Jones WD, Fairlie DP, Tanzi RE, Bush AI (2000) Characterization of copper interactions with alzheimer amyloid beta peptides: identification of an attomolar-affinity copper binding site on amyloid beta1–42. J Neurochem 75:1219–1233. CrossRef Medline

Ayton S, Lei P, Bush AI (2013) Metallostasis in Alzheimer's disease. Free Radic Biol Med 62:76–89. CrossRef Medline

Beyer N, Coulson DT, Heggarty S, Ravid R, Hellemans J, Irvine GB, Johnston JA (2012) Zinc transporter mRNA levels in Alzheimer's disease postmortem brain. J Alzheimers Dis 29:863–873. CrossRef Medline

Bush AI (2013) The metal theory of Alzheimer's disease. J Alzheimers Dis 33 [Suppl 1]:S277–S281.

Bush AI, Pettingell WH, Multhaup G, Paradis M, Vonsattel JP, Gusella JF, Beyreuther K, Masters CL, Tanzi RE (1994) Rapid induction of Alzheimer A beta amyloid formation by zinc. Science 265:1464–1467. CrossRef Medline

Cirrito JR, May PC, O'Dell MA, Taylor JW, Parsadanian M, Cramer JW, Audia JE, Nissen JS, Bales KR, Paul SM, DeMattos RB, Holtzman DM (2003) In vivo assessment of brain interstitial fluid with microdialysis reveals plaque-associated changes in amyloid-β metabolism and half-life. J Neurosci 23:8844–8853. Medline

Cirrito JR, Yamada KA, Finn MB, Sloviter RS, Bales KR, May PC, Schoepp DD, Paul SM, Mennerick S, Holtzman DM (2005) Synaptic activity regulates interstitial fluid amyloid-beta levels in vivo. Neuron 48:913–922. CrossRef Medline

Colvin RA, Bush AI, Volitakis I, Fontaine CP, Thomas D, Kikuchi K, Holmes

WR (2008) Insights into Zn^{2+} homeostasis in neurons from experimental and modeling studies. Am J Physiol Cell Physiol 294:C726–C742. CrossRef Medline

Faux NG, Ritchie CW, Gunn A, Rembach A, Tsatsanis A, Bedo J, Harrison J, Lannfelt L, Blennow K, Zetterberg H, Ingelsson M, Masters CL, Tanzi RE, Cummings JL, Herd CM, Bush AI (2010) PBT2 rapidly improves cognition in Alzheimer's disease: additional phase II analyses. J Alzheimers Dis 20:509–516. CrossRef Medline

Frederickson CJ, Giblin LJ, Krezel A, McAdoo DJ, Mueller RN, Zeng Y, Balaji RV, Masalha R, Thompson RB, Fierke CA, Sarvey JM, de Valdenebro M, Prough DS, Zornow MH (2006) Concentrations of extracellular free zinc (pZn)e in the central nervous system during simple anesthetization, ischemia and reperfusion. Exp Neurol 198:285–293. CrossRef Medline

Gellein K, Skogholt JH, Aaseth J, Thoresen GB, Lierhagen S, Steinnes E, Syversen T, Flaten TP (2008) Trace elements in cerebrospinal fluid and blood from patients with a rare progressive central and peripheral demyelinating disease. J Neurol Sci 266:70–78. CrossRef Medline

Gu L, Tran J, Jiang L, Guo Z (2016) A new structural model of Alzheimer's Aβ42 fibrils based on electron paramagnetic resonance data and Rosetta modeling. J Struct Biol 194:61–67. CrossRef Medline

Hirano T, Kikuchi K, Urano Y, Nagano T (2002) Improvement and biological applications of fluorescent probes for zinc, ZnAFs. J Am Chem Soc 124:6555–6562. CrossRef Medline

Huang X, Atwood CS, Moir RD, Hartshorn MA, Vonsattel JP, Tanzi RE, Bush AI (1997) Zinc-induced Alzheimer's Abeta1–40 aggregation is mediated by conformational factors. J Biol Chem 272:26464–26470. CrossRef Medline

Kepp KP (2016) Alzheimer's disease due to loss of function: a new synthesis of the available data. Prog Neurobiol 143:36–60. CrossRef Medline

Kim SH, Fraser PE, Westaway D, St George-Hyslop PH, Ehrlich ME, Gandy S (2010) Group II metabotropic glutamate receptor stimulation triggers production and release of Alzheimer's amyloid(beta)42 from isolated intact nerve terminals. J Neurosci 30:3870–3875. CrossRef Medline

Lannfelt L, Blennow K, Zetterberg H, Batsman S, Ames D, Harrison J, Masters CL, Targum S, Bush AI, Murdoch R. Wilson J, Ritchie CW (2008) Safety, efficacy, and biomarker findings of PBT2 in targeting Abeta as a modifying therapy for Alzheimer's disease: a phase IIa, double-blind, randomised, placebo controlled trial. Lancet Neurol 7:779–786. CrossRef Medline

Masuda Y, Uemura S, Ohashi R, Nakanishi A, Takegoshi K, Shimizu T, Shirasawa T, Irie K (2009) Identification of physiological and toxic conformations in Abeta42 aggregates. Chembiochem 10:287–295. CrossRef Medline

Matlack KE, Tardiff DF, Narayan P, Hamamichi S, Caldwell KA, Caldwell GA, Lindquist S (2014) Clioquinol promotes the degradation of metal-dependent amyloid-β (Aβ) oligomers to restore endocytosis and ameliorate Aβ toxicity. Proc Natl Acad Sci U S A 111:4013–4018. CrossRef Medline

Michalke B, Nischwitz V (2010) Review on metal speciation analysis in cerebrospinal fluid-current methods and results: a review. Anal Chim Acta 682:23–36. CrossRef Medline

Morley JE, Farr SA, Banks WA, Johnson SN, Yamada KA, Xu L (2010) A physiological role for amyloid beta protein: enhancement of learning and memory. J Alzheimers Dis 19:441–449. CrossRef Medline

Morrison JH, Hof PR (1997) Life and death of neurons in the aging brain. Science 278:412–419. CrossRef Medline

Motter R, Vigo-Pelfrey C, Kholodenko D, Barbour R, Johnson-Wood K, Galasko D, Chang L, Miller B, Clark C, Green R (1995) Reduction of beta-amyloid peptide42 in the cerebrospinal fluid of patients with Alzheimer's disease Ann Neurol 38:643–648. CrossRef Medline

Mucke L, Masliah E, Yu GQ, Mallory M, Rockenstein EM, Tatsuno G, Hu K, Kholodenko D, Johnson-Wood K, McConlogue L (2000) High-level neuronal expression of abeta 1–42 in wild-type human amyloid protein precursor transgenic mice: synaptotoxicity without plaque formation. J Neurosci 20:4050–4058. Medline

Nestor PJ, Scheltens P, Hodges JR (2004) Advances in the early detection of Alzheimer's disease. Nat Med 10 [Suppl] S34–S41.

Perrin RJ, Fagan AM, Holtzman DM (2009) Multimodal techniques for diagnosis and prognosis of Alzheimer's disease. Nature 461:916–922. CrossRef Medline

Puzzo D, Privitera L, Leznik E, Fà M, Staniszewski A, Palmeri A, Arancio O (2008) Picomolar amyloid-beta positively modulates synaptic plasticity and memory in hippocampus. J Neurosci 28:14537–14545. CrossRef Medline

Puzzo D, Privitera L, Fà M, Staniszewski A, Hashimoto G, Aziz F, Sakurai M, Ribe EM, Troy CM, Mercken M, Jung SS, Palmeri A, Arancio O (2011) Endogenous amyloid-β is necessary for hippocampal synaptic plasticity and memory. Ann Neurol 69:819–830. CrossRef Medline

Puzzo D, Privitera L, Palmeri A (2012) Hormetic effect of amyloid-β peptide in synaptic plasticity and memory. Neurobiol Aging 33:1484.e15–24. CrossRef Medline

Querfurth HW, LaFerla FM (2010) Alzheimer's disease. N Engl J Med 362:329–344. CrossRef Medline

Rammes G, Hasenjäger A, Sroka-Saidi K, Deussing JM, Parsons CG (2011) Therapeutic significance of NR2B-containing NMDA receptors and mGluR5 metabotropic glutamate receptors in mediating the synaptotoxic effects of β-amyloid oligomers on long-term potentiation (LTP) in murine hippocampal slices. Neuropharmacology 60:982–990. CrossRef Medline

Schoonenboom NS, Mulder C, Van Kamp GJ, Mehta SP, Scheltens P, Blankenstein MA, Mehta PD (2005) Amyloid beta 38, 40, and 42 species in cerebrospinal fluid: more of the same? Ann Neurol 58:139–142. CrossRef Medline

Sensi SL, Canzoniero LM, Yu SP, Ying HS, Koh JY, Kerchner GA, Choi DW (1997) Measurement of intracellular free zinc in living cortical neurons: routes of entry. J Neurosci 17:9554–9564. Medline

Sindreu CB, Varoqui H, Erickson JD, Pérez-Clausell J (2003) Boutons containing vesicular zinc define a subpopulation of synapses with low AMPAR content in rat hippocampus. Cereb Cortex 13:823–829. CrossRef Medline

Suzuki M, Fujise Y, Tsuchiya Y, Tamano H, Takeda A (2015) Excess influx of Zn^{2+} into dentate granule cells affects object recognition memory via attenuated LTP. Neurochem Int 87:60–65. CrossRef Medline

Syme CD, Viles JH (2006) Solution 1H NMR investigation of Zn^{2+} and Cd^{2+} binding to amyloid-beta peptide (Abeta) of Alzheimer's disease. Biochim Biophys Acta 1764:246–256. CrossRef Medline

Takeda A, Tamano H (2016) Insight into cognitive decline from Zn^{2+} dynamics through extracellular signaling of glutamate and glucocorticoids. Arch Biochem Biophys 611:93–99. CrossRef Medline

Takeda A, Nakamura M, Fujii H, Uematsu C, Minamino T, Adlard PA, Bush AI, Tamano H (2014a) Amyloid β-mediated Zn^{2+} influx into dentate granule cells transiently induces a short-term cognitive deficit. PLoS One 9:e115923. CrossRef Medline

Takeda A, Tamano H, Ogawa T, Takada S, Nakamura M, Fujii H, Ando M (2014b) Intracellular Zn^{2+} signaling in the dentate gyrus is required for object recognition memory. Hippocampus 24:1404–1412. CrossRef Medline

Takeda A, Koike Y, Osaw M, Tamano H (2017) Characteristic of extracellular Zn^{2+} influx in the middle-aged dentate gyrus and its involvement in attenuation of LTP. Mol Neurobiol. Advance online publication. Retrieved Mar. 13, 2017. doi: 10.1007/s12035–017-0472-z. CrossRef Medline

Tõugu V, Karafin A, Palumaa P (2008) Binding of zinc(II) and copper(II) to the full-length Alzheimer's amyloid-beta peptide. J Neurochem 104:1249–1259. CrossRef Medline

Ueno S, Tsukamoto M, Hirano T, Kikuchi K, Yamada MK, Nishiyama N, Nagano T, Matsuki N, Ikegaya Y (2002) Mossy fiber Zn^{2+} spillover modulates heterosynaptic *N*-methyl-*D*-aspartate receptor activity in hippocampal CA3 circuits. J Cell Biol 158:215–220. CrossRef Medline

Wang T, Wang CY, Shan ZY, Teng WP, Wang ZY (2012) Clioquinol reduces zinc accumulation in neuritic plaques and inhibits the amyloidogenic pathway in AβPP/PS1 transgenic mouse brain. J Alzheimers Dis 29:549–559. CrossRef Medline

Xiao Y, Ma B, McElheny D, Parthasarathy S, Long F, Hoshi M, Nussinov R, Ishii Y (2015) Aβ(1–42) fibril structure illuminates self-recognition and replication of amyloid in Alzheimer's disease. Nat Struct Mol Biol 22:499–505. CrossRef Medline

Zhang LH, Wang X, Stoltenberg M, Danscher G, Huang L, Wang ZY (2008) Abundant expression of zinc transporters in the amyloid plaques of Alzheimer's disease brain. Brain Res Bull 77:55–60. CrossRef Medline